

## Synthesis and characterization of ZrO<sub>2</sub>: MgO thin films by plasma of R.F. magnetron sputtering

Zainb Mohammed  
zainabqusim139@yahoo.com

Souad Khalil  
rahf\_mutter@yahoo.com

Mahdi Mutter  
Ministry of Science and Technology, mahdimutter@yahoo.com

Follow this and additional works at: <https://kijoms.uokerbala.edu.iq/home>



Part of the [Physics Commons](#)

### Recommended Citation

Mohammed, Zainb; Khalil, Souad; and Mutter, Mahdi (2019) "Synthesis and characterization of ZrO<sub>2</sub>: MgO thin films by plasma of R.F. magnetron sputtering," *Karbala International Journal of Modern Science*: Vol. 5 : Iss. 1 , Article 3. Available at: <https://doi.org/10.33640/2405-609X.1064>

This Research Paper is brought to you for free and open access by Karbala International Journal of Modern Science. It has been accepted for inclusion in Karbala International Journal of Modern Science by an authorized editor of Karbala International Journal of Modern Science. For more information, please contact [abdulateef1962@gmail.com](mailto:abdulateef1962@gmail.com).

---

## Synthesis and characterization of ZrO<sub>2</sub>: MgO thin films by plasma of R.F. magnetron sputtering

### Abstract

The aim of this work is to prepare thin composite films from zirconia (ZrO<sub>2</sub>) and magnesia (MgO) on to glass basis by plasma of R.F. magnetron sputtering as well as recognize their structural and optical properties. It also aims to study the effect of thermal processing at 450 °C in two hours duration. The structural properties are measured by X-ray diffraction (XRD), scanning electron microscopy (SEM) and atomic force microscopy (AFM). The chemical analysis for the ready films had been studied using energy dispersive x-ray (EDX). The optical properties had been studied by using UV-Visible spectroscopy. Results show that the grain size of the ready films, which were thermally treated, was between 18.44 and 33.22 nm and the crystalline structure was a monoclinic phase with almost a spherical form for the grains. There was a homogenous distribution for all the ready films. The energy gaps decreased from 3.9 to 3.09 eV with an increase in the doping ratios.

### Keywords

ZrO<sub>2</sub>: MgO thin films, plasma sputtering technique, structural properties, optical properties and thermal effect

### Creative Commons License



This work is licensed under a [Creative Commons Attribution-Noncommercial-No Derivative Works 4.0 License](https://creativecommons.org/licenses/by-nc-nd/4.0/).

## 1. Introduction

The thin films of oxide mater are attracting in an expanding interest due to of their important use as the material with high dielectric properties for manufacturing of the film capacitors and as a thin layer with high chemical stability at making of multi-layers [1]. Nowadays, nano-scaled zirconia-magnesia ceramics production is among the most critical classes of strong impetuses utilized as an active phase; they have pulled in a lot of consideration because of such properties as amazing chemical and thermal stability, high porosity and substantial surface area [2,3]. The zirconia ( $ZrO_2$ ) is considered one of the important materials in the industrial and advanced materials sciences. This is due to its unique properties, which included good refractions, chemical resistance, excellent mechanical strength, low thermal conductivity at high temperature with high thermal conductivity, and its high thermal stability [4,5]. There is a range of industrial application for the  $ZrO_2$ . It is used in ceramics, gas sensors, batteries, corrosion resistance, thermal barrier, coating fuel cell in Industrie sand as catalysts [6–8]. There are three phases for pure zirconia: the monoclinic, tetragonal and cubic. The monoclinic is thermally stable at room temperature, but at 1170 °C, it is transferred to the tetragonal phase. This means that the tetragonal and cubic phases are the only phases which could exist at high temperatures. These two phases, the tetragonal and the cubic, are unstable at room temperature. Due to many applications of these two phases and to increase the stability, we use other oxides, the tetragonal and the cubic [9]. These oxides include  $Y_2O_3$ , MgO and CaO. Minimizing the grain size or particle size to the nanoscale, we have to increase the stability of these two phases [10,11]. Adding MgO to the zirconia gives an improvement to its physical properties as far as thermal stabilization and increasing the positive characteristics of the zirconia are concerned [12,13]. (see Tables 1)

In this study, we aim to improve the characterization of  $ZrO_2$  by adding MgO. The technique of radio frequency magnetron plasma sputtering has been used to prepare magnesia as a stabilizer for the nanoparticles of the zirconia. The targets have been made in the laboratory with doping and composite ratios of 6–10% as a weight ratio of the zirconia, which formed the matrix in this composition. For this composite, we

calculated the relevant structural and optical properties as will be shown below.

## 2. Materials & method

### 2.1. Preparation of $ZrO_2$ : MgO nanocomposites

The raw materials in this work are manufactured by Changsha Santech, China, for the  $ZrO_2$  powder with purity 99.94% and particles grain size ( $30 \pm 5$  nm), while the MgO powders are made by Nanjing Nano Technology, China with purity 99.9% and particles grain size 30 nm–40 nm. The  $ZrO_2$ : MgO nanocomposites have been prepared by using the plasma of R.F. magnetron sputtering technique with different doping ratio for MgO, the ratios were (6, 8 and 10)% from the  $ZrO_2$  weight. The target used in sputtering were of 50 mm in diameter and a thickness of 3 mm. A hydraulic press has been used to press with 10 tons. Then, thermal processing (sintering) has been made to the target at 850 °C, and after that, the process of grinding and polishing has been done. The system used in the preparation was the American type CRC, Compact Research Coater-600-Torr. Glass bases were as substrate. The glass bases were treated by cleaning and processing rules. Thermal processing (annealing) was conducted, after preparing the samples, at 450 °C for 2 h.

### 2.2. Materials characterization

The structural properties of the prepared films have been studied using X-ray diffraction (XRD). The XRD type Shimadzu (Japanese made) del: XRD 6000 using  $CuK\alpha$  ( $\lambda = 0.154$  nm) radiation, with diffraction angle between 20° and 80°. The scanning electron microscopy (SEM) was type JEOL.JSM-67001, made in Germany. The energy dispersive (EDX) was with 15 kV. The study of the surface has been done using atomic force microscopy (AFM), and it was type SPM Milegra NT. MIOT, Russian made. Before taking the samples' reputation by scanning electron microscopy, a layer of gold was deposited on the prepared films using the technique of sputtering with a system type of DST3, model, nanostructure coating Co made in Iran. The optical characteristic has been studied using UV–Visible Recording spectroscopy-type, made in Japan. It has a range of wavelength 200–1100 nm.

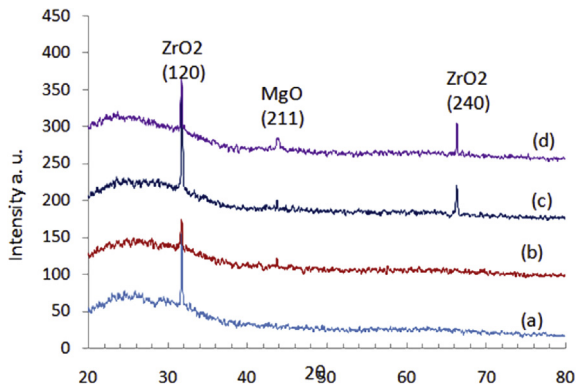


Fig. 1. The typical XRD analysis results of  $ZrO_2:MgO$  and thermal treated, (a)  $ZrO_2$  pure, (b)  $ZrO_2:6\%MgO$ , (c)  $ZrO_2:8\%MgO$ , (d)  $ZrO_2:10\%MgO$ .

### 3. Results and discussion

Results of testing, using x-ray diffraction and after comparing with the international card of  $ZrO_2$  (JCPDs Card No. 00-041-1746) and the international card of  $MgO$  (JCPDs card No. 77-2364), showed that prepared films ( $ZrO_2:MgO$ ) have a multi-crystal composite of the monoclinic phase. The common direction of crystallization is (120) as in Fig. 1 which represent the prepared films with thermal processing at  $450^\circ C$  for 2 h. The results showed that the crystal composite of

the prepared films might be affected by the doping of  $MgO$ . This happens with reverse doped films and undoped films. Thermally processed films exist on the monoclinic phase composite. It is also noticed that there is a change in the peak position pattern diffraction shown in Fig. 1. This is due to being dropped by magnesium oxide. One of the important notifications about diffraction pattern is that the crystallization degree (N), which was calculated [14,15] 0.010501 to 0.016813, is increasing with the increase of the ratio of doping for the samples  $ZrO_2$  pure and  $ZrO_2:10\%MgO$ , while the samples  $ZrO_2:6\%MgO$  was 0.004039 and  $ZrO_2:8\%MgO$  was 0.001342, that the deuced spacing is decreasing with the increasing of dropping vain. This is due to the size of the magnesium ion, which was added, is less than that of the size of zirconium ion in the original material [16]. The crystal size of all the prepared films was calculated [15], the value was (46.411 nm) for the  $ZrO_2$  pure sample, and the other samples values were close, this is because of the effect of the thermal processing, which kept for the stability of the material. The dislocation density was calculated [14]. The dislocation density increased from  $4 \times 10^{-4}$  lines/ $m^2$  for  $ZrO_2$  pure to  $4-6 \times 10^{-4}$  lines/ $m^2$  for the  $ZrO_2:10\%MgO$ .

Fig. 2 represents the image of the SEM for the prepared samples. The size of this image was 500 nm.

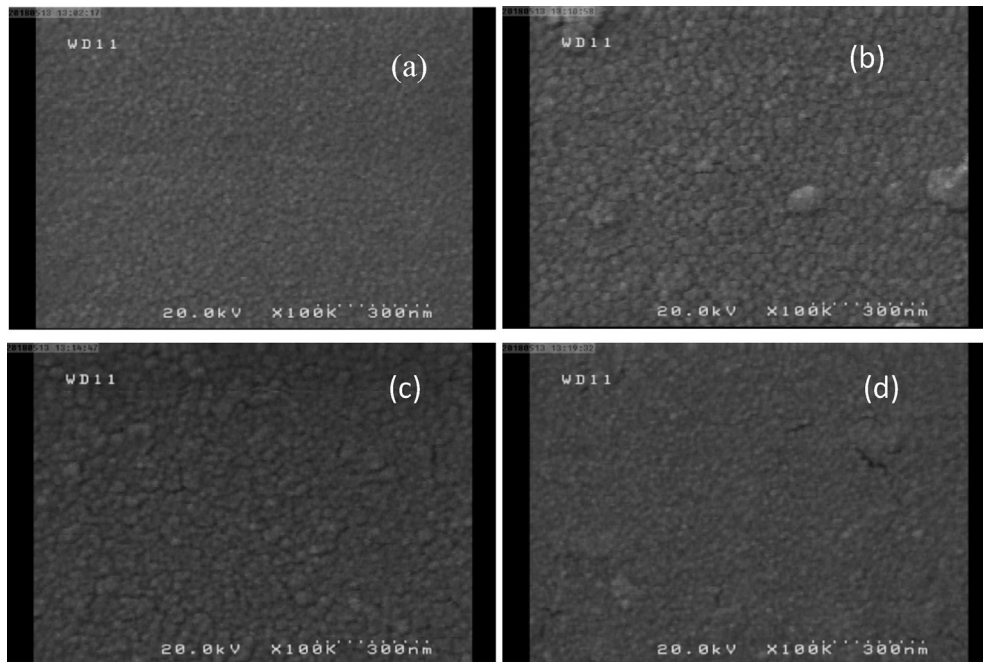


Fig. 2. Typical top view SEM image of  $ZrO_2:MgO$  thin films and thermal treated, (a)  $ZrO_2$  pure, (b)  $ZrO_2:6\%MgO$ , (c)  $ZrO_2:8\%MgO$ , (d)  $ZrO_2:10\%MgO$ .

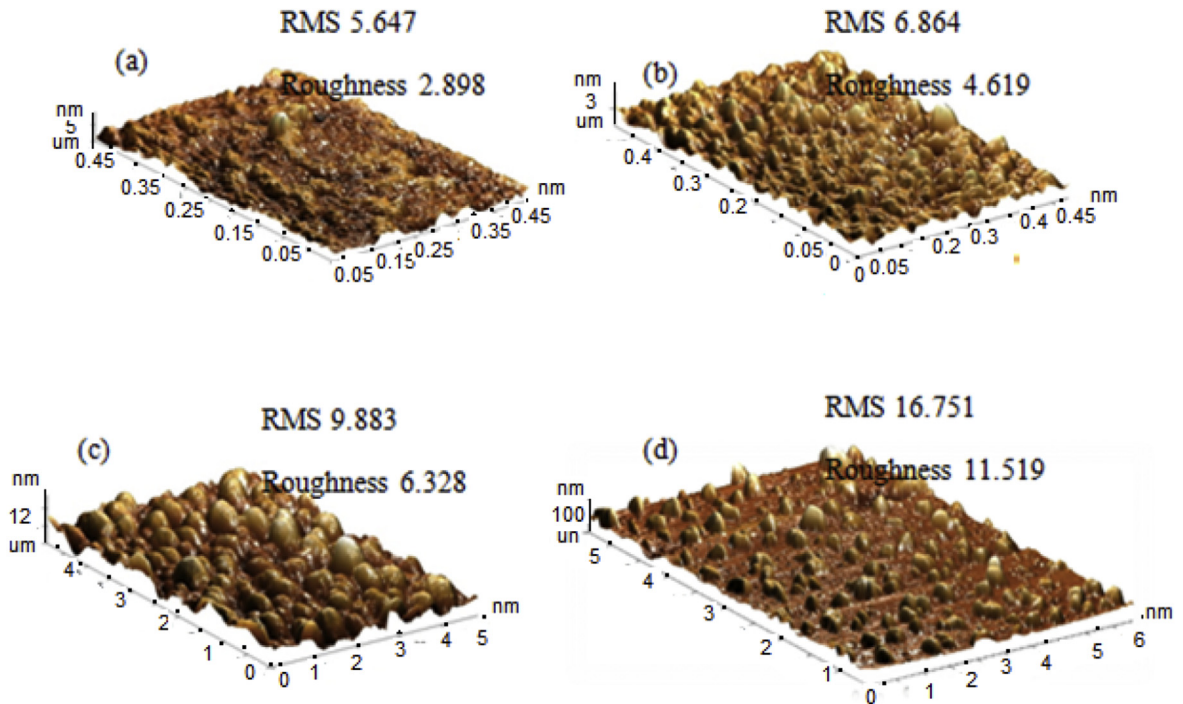


Fig. 3. Indicator AFM image and thermal treated, (a)  $ZrO_2$  pure, (b)  $ZrO_2:6\%MgO$ , (c)  $ZrO_2:8\%MgO$ , (d)  $ZrO_2:10\%MgO$ .

This was for the thermally processed samples at  $450^\circ C$ . The images show a homogenous distribution of the grains and that of spiral form with other different forms with low ratios. The grain size rate for the first sample  $ZrO_2$  pure was 28.25 nm. The second sample  $ZrO_2: 6\% MgO$  was 23.21 nm. The third sample  $ZrO_2: 8\% MgO$  was 33.22 nm. The fourth sample  $ZrO_2: 10\% MgO$  was 18.44 nm. The reason for the high homogeneity in gains distribution on the surface is due to the regularity in the sputtering ions flux when preparing samples; this gives the sample a surface homogeneity. There was a slight difference between the  $ZrO_2: 6\% MgO$  sample and the  $ZrO_2: 8\% MgO$ . There was accumulation for some particles though there was

homogeneity on the surface. The reason may be related to the slight difference in some circumstances of operating.

Fig. 3 shows images of AFM in three dimensions of ready samples with thermal processing at  $450^\circ C$ . The survey process was made with  $2 \times 2 \mu m$  in dimension. The grain size distribution was increased from 13.2 nm to 36.3 nm within increase in the doping ratios of MgO. The roughness also increased from 2.88 nm of the  $ZrO_2$  pure sample to 11.519 nm of the  $ZrO_2:10\% MgO$  sample. The square root values of the RMS (Roughness Medium Square) was 5.647 nm for  $ZrO_2$  pure sample and increasing to 16.751 nm for the  $ZrO_2:10\% MgO$  sample as it is shown in Table 2. This increase in

Table 1  
Structural properties for prepared samples with annealing processing.

Samples	Average crystallite size(D) nm	Number of crystalline No	$\delta$ lins/m <sup>2</sup>
$ZrO_2$ pure	46.411	0.001829	0.00046
$ZrO_2:6\%MgO$	30.953	0.006360	0.00140
	20.240	0.022747	0.00271
	26.655	0.007152	0.00141
$ZrO_2:8\%MgO$	46.421	0.001354	0.00046
	20.251	0.016308	0.00271
	24.411	0.001723	0.00460
$ZrO_2:10\%MgO$	19.248	0.024155	0.00270
	25.312	0.010621	0.00145

Table 2  
Parameters value of AFM image for ready samples.

Samples	Roughness nm	RMS nm	Distribution of grain size nm
ZrO <sub>2</sub>	2.898	5.647	13.2
ZrO <sub>2</sub> :6%MgO	4.619	6.864	14.7
ZrO <sub>2</sub> :8%MgO	6.328	9.883	29.5
ZrO <sub>2</sub> :10%MgO	11.519	16.751	36.3

the surface roughness could be related to the coalescence of the film particles as a result of the thermal processing. We also notice that from the results of the Atomic Force Microscope in Fig. 4, surface of the samples.

Fig. 5 represents the dispersive analysis of the x-ray energy of the ready samples. It shows the chemical analysis of the ready film components which are under thermal processing at 450 °C. Table 3 shows the weight and atomic percentage for the positive ion (Zr, Mg) and negative ions (O). The results show that the phase of the prepared films is the only phase noticed and there is no development of another phase. This shows the purity of these films and the quality of the raw materials

which were used as well as the accuracy and clearness in the operation of the sputtering system.

Fig. 6 shows the prepared films transmittable for the wavelengths from the infrared area to the visible light to the ultraviolet for all samples thermally treated. Results showed a relative spacing and separation for the spectrum lines of the prepared samples as in Fig. 6. Results showed the transmittable increases for the range of wavelength 300–500 nm before it reaches stability at the transmissibility of 18% of the energy of the fallen beam. This happens until it decreases at a wavelength of 1000 nm except for the sample of ZrO<sub>2</sub>:10%MgO, which has an increase in permeability from 200 to 300 nm then is stable after the wavelength 300 nm with transmissibility of 1%. This behavior of this sample is related to the deformities by the drain and the fallen photon energy, which is affected by the samples' homogeneity [17]. The absorption results are shown in Fig. 7. We notice that an absorption decreases as much as the wavelength of the fallen beam increases. This means that the energy of the fallen photon could not transfer the electrons from the parity beams to the conduction beams. The fallen photon

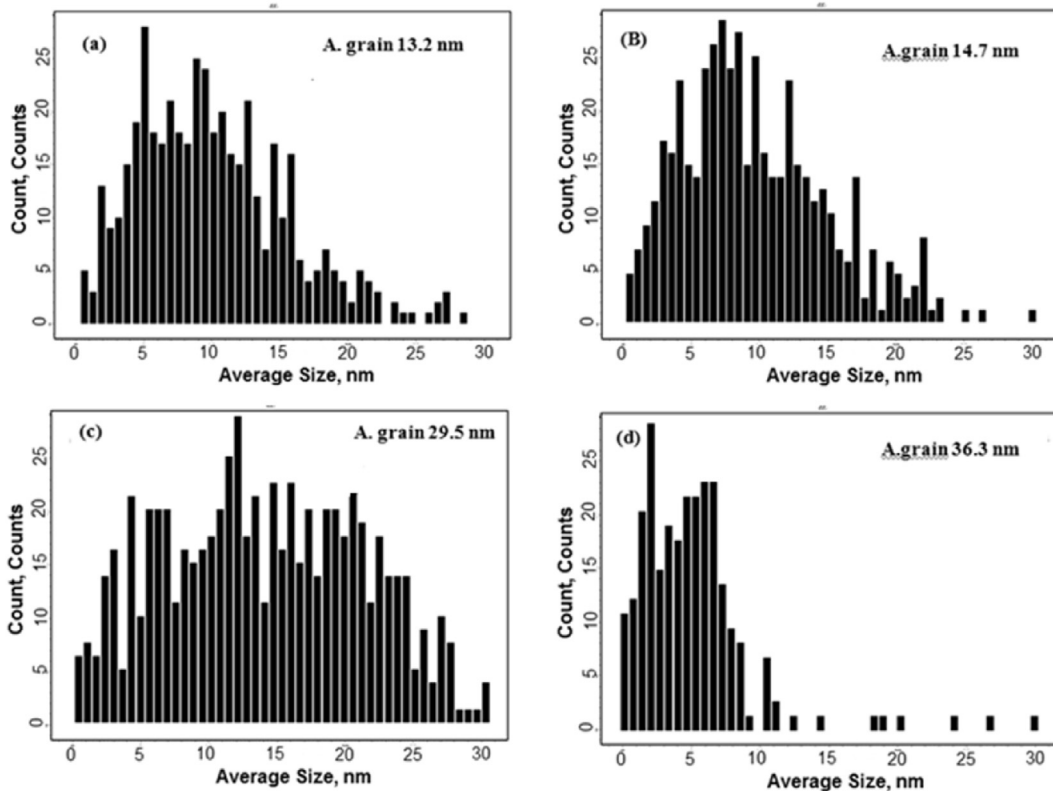


Fig. 4. Corresponding histograms of the surface particle size distribution for ZrO<sub>2</sub>:MgO thin films: (a) ZrO<sub>2</sub> pure, (b) ZrO<sub>2</sub>:6%MgO, (c) ZrO<sub>2</sub>:8%MgO and (d) ZrO<sub>2</sub>:10%MgO; where A.: average.

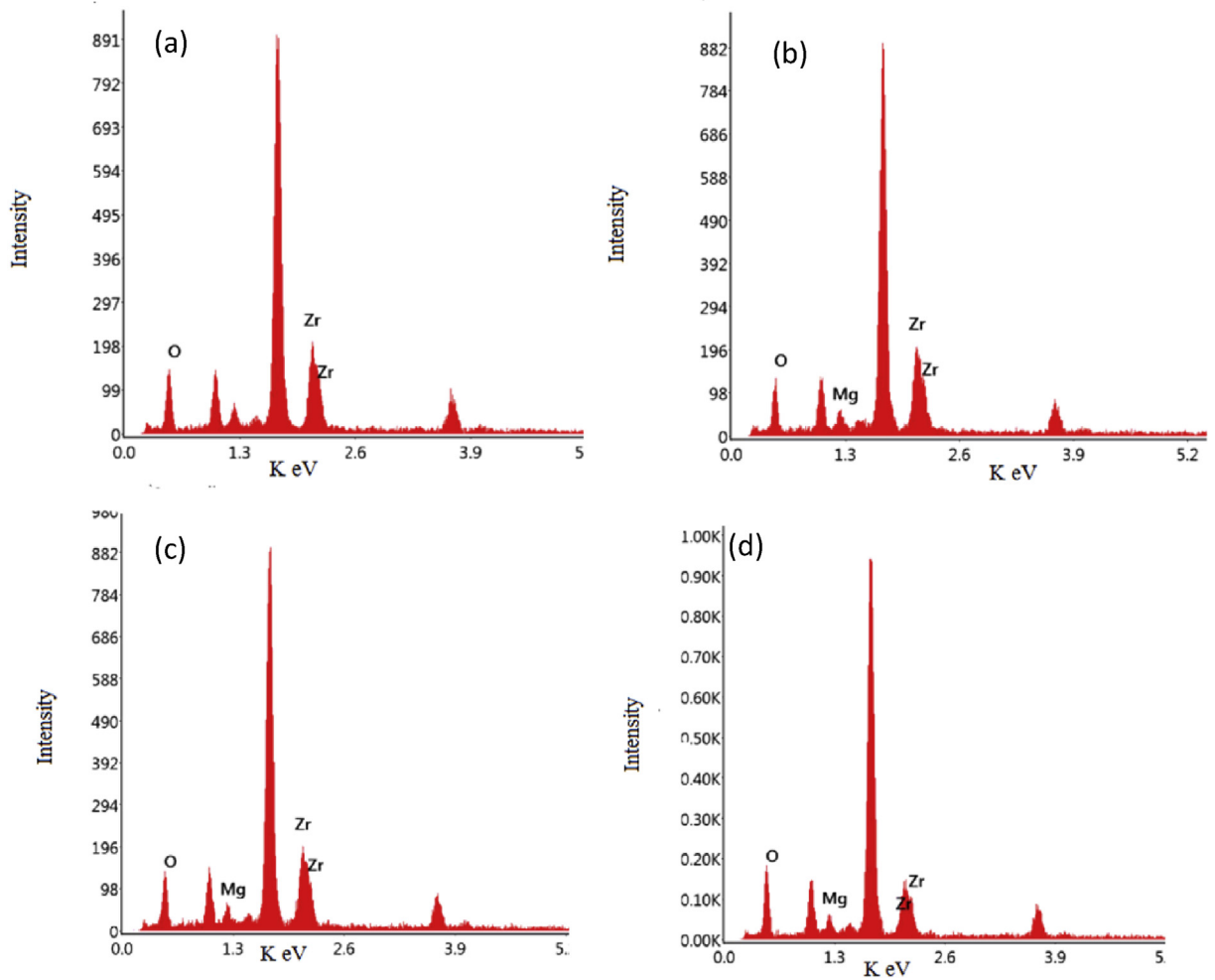


Fig. 5. The typical EDX spectra of ZrO<sub>2</sub>:MgO thin films and thermal treated: (a) ZrO<sub>2</sub> pure, (b) ZrO<sub>2</sub>:6%MgO, (c) ZrO<sub>2</sub>:8%MgO, (d) ZrO<sub>2</sub>:10% MgO.

Table 3  
Analysis of chemical of ready samples with thermal processing.

Samples	Element	Energy level	Weight Percentage %	Atomic Percentage %	Error
ZrO <sub>2</sub> pure	O	K	71.3	93.4	11.3
	Zr	L	28.7	6.6	2.9
ZrO <sub>2</sub> :6%MgO	O	K	54.6	79.1	12.3
	Mg	K	13.4	12.7	15
ZrO <sub>2</sub> :8%MgO	Zr	L	32	8.1	2.8
	O	K	57.4	18.1	11.9
	Mg	K	12.1	11.3	16.5
ZrO <sub>2</sub> :10%MgO	Zr	L	30.5	7.6	2.9
	O	K	64.5	82.3	10.4
	Mg	K	15.9	13.3	13.6
	Zr	L	19.6	4.4	2.9

energy is less than the optical energy gap. The sudden absorption increase at the short wavelengths is related to absorbing that energy. The electrons absorbed this energy to cross the parity area into the conduction

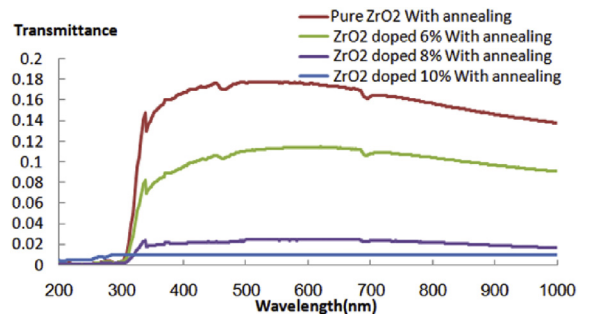


Fig. 6. UV–visible transmittance of ZrO<sub>2</sub>: MgO thin films and thermal treated.

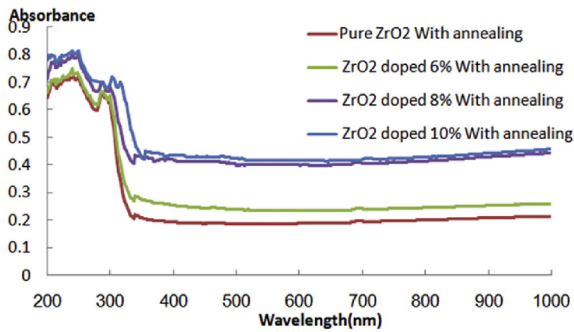


Fig. 7. UV–visible absorption of ZrO<sub>2</sub>: MgO thin films and thermal treated.

beams [18,19]. This area represents the absorption edge between 340 nm, and it is increased for some samples to be 350 nm. The energy gap of the prepared films that are under thermal processing has been calculated in Fig. 8. The energy gap decreased with increase in the ratio of doping. The energy gaps of the prepared films for the direct transformation that are permitted have been calculated using the following equation [17]:

$$(\alpha \cdot hv)^2 = p^2(hv - E_g) \text{ where } (\alpha \cdot hv)^2 = 0 \therefore E_g = hv$$

In comparison with other studies such as the researcher (V. Sunke et al., 2018) [20], we note that the addition of MgO has greatly improved the absorption and transmittance spectroscopy, where the stability of the incident photons have become much more stable and the energy gaps have also decreased to (3.6–3.9) eV compared to the work of the researcher (V. Sunke et al., 2018) Which got the energy gaps about 5.66 eV–5.78 eV.

#### 4. Conclusion

A composite of ZrO<sub>2</sub>: MgO thin films have been prepared, at different ratios of MgO successfully by using radio frequencies of plasma magnetron sputtering. The structural tests in the XRD showed that the structure of the prepared films, which are thermally processed at 450 °C was a monoclinic phase. The SEM confirmed that the shape of the grain is spherical with a grain size between 18.44 and 33.22 nm for the

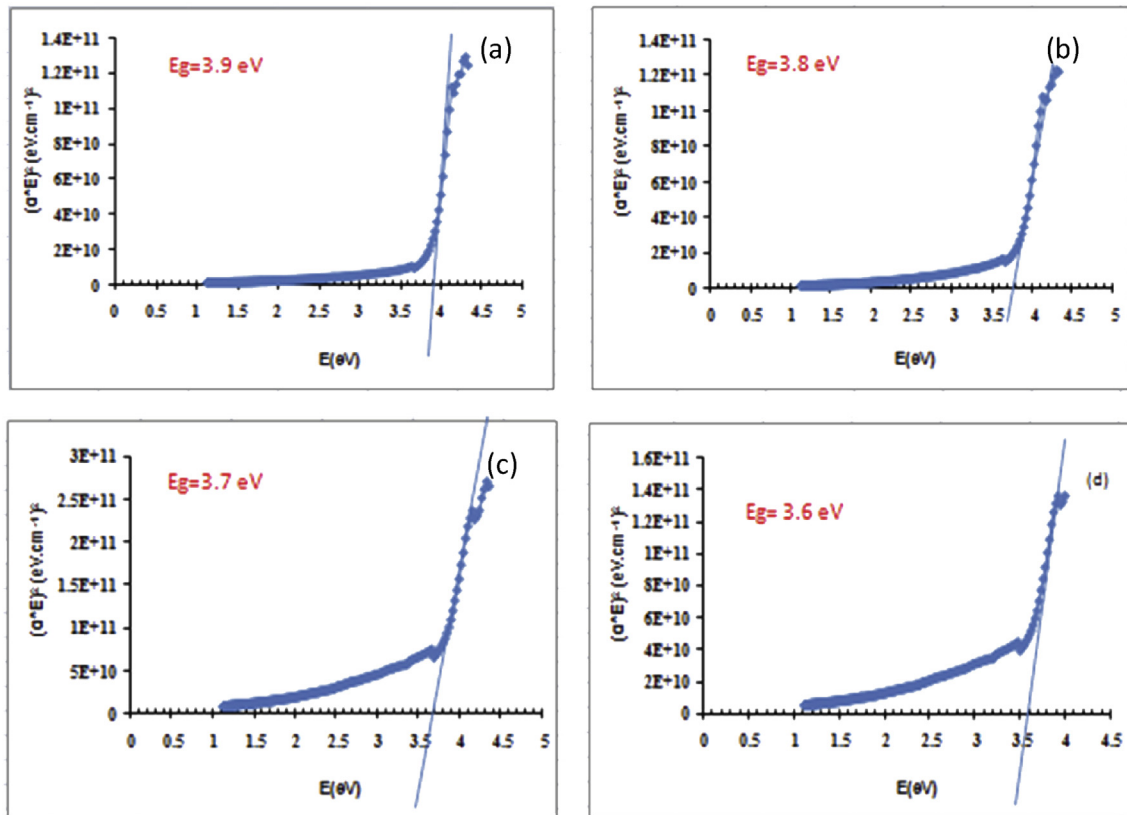


Fig. 8. Energy gap of ZrO<sub>2</sub>:MgO thin films and thermal treated: (a) ZrO<sub>2</sub> pure, (b) ZrO<sub>2</sub>:6%MgO, (c) ZrO<sub>2</sub>:8%MgO, (d) ZrO<sub>2</sub>:10%MgO.

thermally processed samples and 20.77 nm. The AFM tests confirmed that the homogenous distribution surface of the grains and the grain distribution size for the surface were 13.2 and 36.3 nm for the thermally processed samples.

### Conflicts of interest

The authors declare that they have no conflict of interest.

### References

- [1] A.K. Elttayef, A.K. Abbas, G.H. Neema, Nanostructural properties of zirconium oxide thin films prepared by magnetron sputtering, *Int. J. Appl. Innovat. Eng. Manag. (IJAIEM)* 4 (2015) 40–43.
- [2] S. Zinatloo, M. Salavati-Niasavi, Synthesis of pure nanocrystalline ZrO<sub>2</sub> via a simple, sonochemical- assisted route, *J. Ind. Eng. Chem.* 20 (2014) 3313–3319.
- [3] F. Davar, N. Shayan, A. Hojjati-Najafabadi, V. Sabaghi, S. Hasani, Development of ZrO<sub>2</sub>-MgO nanocomposite powders by the modified sol-gel method, *Int. J. Appl. Ceram. Technol.* (2016) 1–9.
- [4] S. Zinatloo-Ajabshir, M. Salavati-Niasari, Facile route to synthesize zirconium dioxide (ZrO<sub>2</sub>) nanostructures: structural, optical and photocatalytic studies, *J. Mol. Liq.* 216 (2016) 545–551.
- [5] M. Gawande, A. Rathi, P. Branco, Nano MgO-ZrO<sub>2</sub> mixed metal oxide, characterization by SIMS and application in the reduction of carbonyl compounds and in multicomponent reaction, *RSC Adv.* 3 (2013) 3611–3617.
- [6] G. Guo, Y. Chen, A nearly pure monoclinic nanocrystalline zirconia, *J. Solid State Chem.* 178 (5) (2005) 1675–1682.
- [7] M. Hajizadeh, R. Razali, M. Khajclokzay, Optimizing Sol-Gel synthesis of magnesia-stabilized zirconia (MSZ) nanoparticles using the Taguchi robust design for thermal barrier coatings (TBCs) application, *J. Sol. Gel Sci. Technol.* 73 (73) (2015) 227–241.
- [8] G. Pratap, D. Kajale, V. Patil, G. Patil, G. Jain, Synthesis and nanostructure ZrO<sub>2</sub> for gas sensing application, *J. Smart Sens. Intell. Syst.* 5 (3) (2012) 673–683.
- [9] S. Deshmukh, R. Bari, Nanostructure ZrO<sub>2</sub> thin films deposited by spray pyrolysis techniques, *Int. Lett. Chem. Phys. Astron.* 56 (2015) 120–130.
- [10] M. Hajizadeh, R. Razavi, M. Loghman, Synthesis and characterization of transformable tetragonal YSZ nanopowders by means of perching method for thermal barrier coating (TBC) application, *J. Sol. Gel Sci. Technol.* 70 (1) (2014) 6–13.
- [11] M. Hajizadeh, R. Razavi, A. Ghasemi, Synthesis and characterization of ceria-yttria Co-stabilized zirconia (CZ) nanoparticles by Sol-Gel process for thermal barrier coating (TBC), *J. Sol. Gel Sci. Technol.* 749 (3) (2015) 603–612.
- [12] J.D. Philip, A. Aujla, K.H. Grant, A.G. Brundle, M.R. Thompson, Practical use of metal oxide semiconductor gas sensors for measuring nitrogen dioxide and ozone in an urban environment, *Sensors* 17 (1653) (2017) 1–25.
- [13] P. Amezaga, W. Antunez, J. Gozalca, J. Saen2, Microstructure properties of multi-nano layered YSZ thin film, *J. Alloy. Comp.* 495 (2) (2016) G29–G33.
- [14] B. Cullity, S. Stock, Elements of X-Ray Diffraction, third ed., Prentice Hall, New York, 2001.
- [15] M. Dhanam, R. Prabhuandand, P. Manoj, Investigations on chemical path deposited Cadmium thin films, *Mater. Chem. Phys.* 107 (2008) 289–296.
- [16] M. Loghman- Estarki, R. Razavi, H. Edris, S. Bakshi, H. Janali, Comparison of hot corrosion behavior of nanostructured Sc YSZ and YSZ thermal barrier coating, *Ceram. Int.* 42 (6) (2016) 7432–7439.
- [17] W. Lijian, M. Vasco, T. Shigeng, S. Zheng, Structure and optical properties of ZnO: V thin films with different doping concentrations, *Thin Solid Flim* 517 (2009) 3721–3728.
- [18] K.M. Wong, W. Khan, M. Shoaib, U. Shah, G. Murtaza, Ab Initio investigation of the structural, electronic and optical of the Li<sub>2</sub>In<sub>2</sub>XY<sub>6</sub> (X = Si, Ge; Y = S, Se) compounds, *J. Electron. Mater.* 47 (2018) 566–567.
- [19] K.M. Wong, S.M. Alay-e-Abbas, Y. Fang, A. Shaukat, Y. Lei, Spatial distribution of neutral oxygen vacancies on ZnO nanowire surfaces: an investigation combining confocal microscopy and first-principles calculations, *J. Appl. Phys.* 114 (2013) 034901.
- [20] V. Sunke, G.N. Bukke, U. Suda, Characterisation of nanostructured ZrO<sub>2</sub> thin films formed by DC reactive magnetron sputtering, *J. Nano Res.* 7 (65) (2018) 68.